

- Crowder, B. L. (Ed.) (1973). "Ion Implantation in Semiconductors and Other Materials", (Yorktown Heights, 1972) Plenum Press.
- Crowder, B. L. (Ed.) (1975). "Ion Implantation in Semiconductors and Other Materials", (Osaka, 1974) Plenum Press.
- Dearnaley, G. (1969). *Rep. Prog. Phys.* 32, 405.
- Dearnaley, G., Freeman, J. H., Nelson, R. S. and Stephen, J. (1973). "Ion implantation", North Holland.
- Degen, P. L. (1973). *Phys. Stat. Sol.* A16, 9.
- Eisen, F. H. and Chadderton, L. T. (Eds) (1971). "Ion Implantation" (Proc. 1st Int. Conf.—Thousand Oaks), Gordon and Breach.
- Gibbons, J. F. (1972). *Proc. IEEE*, 60, 1062.
- Mayer, J. W., Eriksson, L. and Davies, J. A. (1970). "Ion Implantation in Semiconductors", Academic Press.
- Mayer, J. W. and Marsh, O. J. (1969). *Applied Solid State Science*, 1, 239.
- Namba, S. (Ed.) (1971). "Ion Implantation in Semiconductors" (Proc. U.S.-Japan Seminar), Japan Soc. for promotion of science, Kyoto.
- Palmer, D. W., Thompson, M. W. and Townsend, P. D. (Eds) (1970). "Atomic Collision Phenomena in Solids", North Holland.
- Picraux, S. T., Eer Nisse, E. P. and Vook, F. L. (Eds) (1974). "Applications of Ion Beams to Metals", Plenum Press.
- Ruge, I. and Graul, J. (Eds) (1971). "Ion Implantation in Semiconductors" (Proc. 2nd Int. Conf.—Garmisch-Partenkirchen), Springer-Verlag.
- Schulz, M. (1974). *Applied Physics*, 4, 91.
- Thompson, M. W. (1969). "Defects and Radiation Damage in Metals", Cambridge University Press.

General References

- Carter, G. and Grant, W. A. (1976). "Ion Implantation in Semiconductors", Arnold.
- Corbett, J. W. and Ianiello, L. C., (Eds) (1972). "Radiation Induced Voids in Metals", U.S.A.E.C. Symp. series 26.
- Friedel, J. (1964). "Dislocations", Addison-Wesley.
- Henderson, B. (1972). "Defects in Crystalline Solids", Arnold.
- Kittel, C. (1971). "Introduction to Solid State Physics", Fourth Edition, Wiley.
- Nabarro, F. R. N. (1967). "Theory of Crystal Dislocations", Oxford University Press.
- Namba, S. and Masusla, K. (1975). *Electronics and Electron Physics*, 37, 264.
- Proc. of Amsterdam Conf. on "Atomic Collisions in Solids" (1976). "Surface Science", to be published.
- Proc. of Warwick Conf. on "Ion Implantation in Semiconductors and Other Materials" (1976), I.O.P.
- "Theory of Imperfect Crystalline Solids (1971). I.A.E.A., Vienna.

THIS MATERIAL MAY BE
PROTECTED BY
COPYRIGHT LAW
(TITLE 17, U.S. CODE)

CHAPTER 2

Ion Ranges in Solids

2.1 PROCESSES OF ENERGY LOSS

If we are to control the properties of ion implanted surfaces then we must understand the mechanisms of energy loss which control the depth distribution of the implant as well as the radiation damage which ensues along the track as energy is transferred to the solid. To do this we consider the scattering events which influence the total path length, the range straggling and the projected depth of the implant in the direction of the original ion beam. The theories contain many assumptions and empirical correction factors so for practical applications one might wish to proceed directly to the widely used range estimates which are those of Lindhard, Scharff and Schiøtt (1963), (LSS). Range-energy tables have been computed from their theory for a variety of ion-solid systems by Johnson and Gibbons (1970) and Smith (1971). A selection of typical data is included in the books by Carter and Colligon (1968), Mayer *et al.* (1970), Dearnaley *et al.* (1973), Wilson and Brewer (1973) and in Appendix I of this present volume.

Calculations of energy deposition with depth into the target material will also give some measure of the radiation damage produced during the implantation. These depth distributions will be discussed in Section 2.12. It should be noted that the stability of the displaced atoms will determine the final state of the radiation damage and this is discussed in greater detail in Chapter 4.

We shall first discuss the derivation of the LSS range theory. The major processes of energy loss are (i) direct collisions between the ion and a screened nucleus, (ii) excitation of electrons bound in the solid and (iii) charge exchange processes between the ion and the atoms of the solid. All three processes are energy dependent and so make different contributions to the energy loss along the path of the ion. For simplicity we will treat the three independently and write a differential energy loss equation as

$$\left(\frac{dE}{dx}\right)_{\text{loss}} = \left(\frac{dE}{dx}\right)_{\text{nuclear}} + \left(\frac{dE}{dx}\right)_{\text{electronic}} + \left(\frac{dE}{dx}\right)_{\text{exchange}}$$

Correlations between the events and the subsequent motion of the displaced atoms will be ignored whilst considering the range of implanted ions. However we must consider movements of the displaced atoms when we discuss radiation damage, as the displaced atoms can in turn impart sufficient energy to cause many further displacements. Fortunately the problem can be treated classically as a scattering event between two ions. In part this is possible because the dominant energy loss, by elastic nuclear collisions, occurs for ions between 5 and 500 keV and also detailed electronic structure effects are lost in amorphous solids because the final range is determined by many individual events. This averaging effect allows us to use the LSS theory for non-crystalline materials. Adjustments to the theory are required when the ion moves nearly parallel to crystal directions. Many crystalline directions act as channels and the ion bounces along with a relatively weak interaction with the walls, however in this instance specific electronic orbitals are involved so electronic shell effects must be considered. The associated reduction in dE/dx frequently produces channelled ranges up to ten times those expected for ions injected in a random direction. Channelling plays a significant role in ion implantation studies and light ion analytical studies of Rutherford backscattering (see Chapter 8).

2.2 CLASSICAL COLLISIONS

In the energy range used for implantation, 5–500 keV, the dominant energy loss is by elastic interactions between the ion and a screened nucleus. The problem is simplified by considering two body events in a centre of mass coordinate system to predict the energy loss, T , the cross section for energy transfer, $d\sigma_{\text{nuclear}}$, and the angle of scattering. The trajectory of the particles for a two body collision event is shown in Fig. 2.1 for a laboratory frame and the equivalent collision in a centre of mass frame is presented in Fig. 2.2. In the laboratory frame the momentum must be $M_1 u_1 = (M_1 + M_2) V_{\text{CM}}$. This is equivalent to moving the particle M_2 in the centre of mass frame at a velocity

$$U_2 = - \frac{M_1 u_1}{(M_1 + M_2)}$$

Since the collision is elastic both energy and momentum are conserved so

$$M_1 U_1^2 + M_2 U_2^2 = M_1 V_1^2 + M_2 V_2^2$$

and

$$M_1 U_1 - M_2 U_2 = M_1 V_1 - M_2 V_2$$

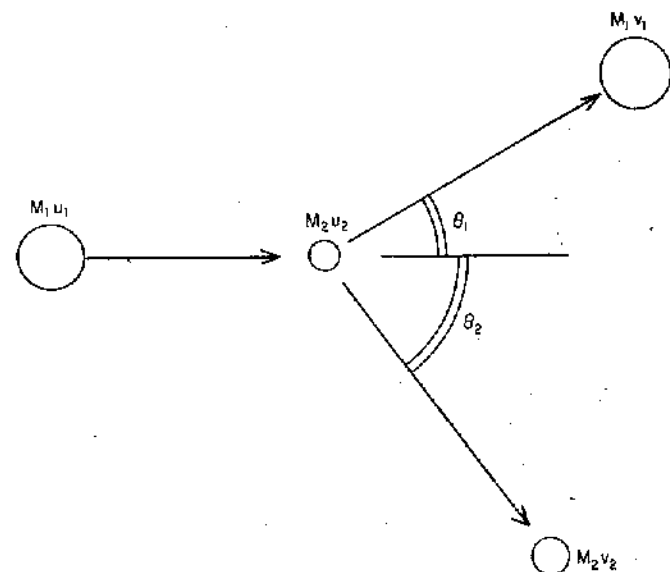


FIG. 2.1. A collision between two particles in a laboratory co-ordinate system.

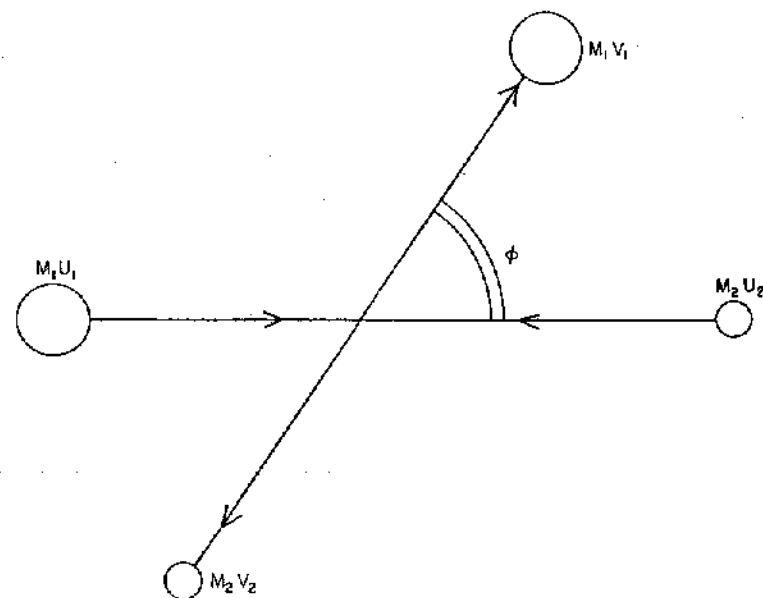


FIG. 2.2. A collision between two particles in a centre of mass frame co-ordinate system.

which implies

$$U_1 = V_1 = \frac{M_2 u_1}{M_1 + M_2}$$

and

$$U_2 = V_2 = \frac{M_1 u_1}{M_1 + M_2}$$

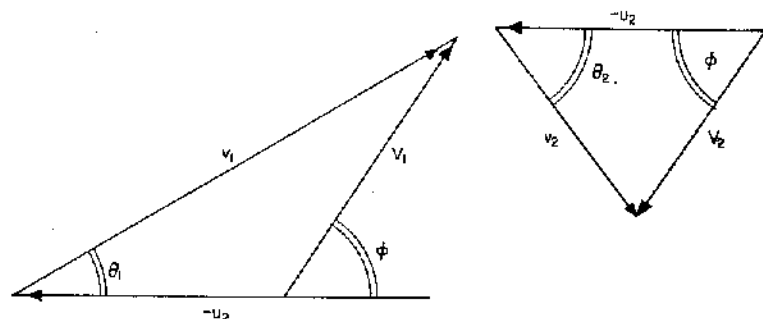


FIG. 2.3. Vector diagrams of the velocities which relate the two co-ordinate systems.

A consideration of vector diagrams, Fig. 2.3, enables us to relate the angles in the two systems by

$$V_2 \cos \phi + V_2 \cos \theta_2 = u_2$$

$$V_2 \sin \phi = V_2 \sin \theta_2$$

which can be reduced to

$$\sin \phi = \tan \theta_2 (1 - \cos \phi).$$

The recoil energy of the struck atom, $E_2 = \frac{1}{2} M_2 v_2^2$ is the energy transferred T , but

$$v_2^2 = 2(1 - \cos \phi) \frac{M_1^2 u_1^2}{(M_1 + M_2)^2}$$

so

$$T = \frac{4M_1 M_2}{(M_1 + M_2)^2} E_1 \sin^2 \left(\frac{\phi}{2} \right).$$

This sets an upper limit for energy transfer in a head-on collision as

$$T_{\max} = \frac{4M_1 M_2}{(M_1 + M_2)^2} E_1.$$

E_1 and T may differ by several orders of magnitude if there is a disparity between M_1 and M_2 and only a small angle collision occurs, it is therefore sensible to ask if a classical approach is justified.

The moving particle has an associated wavelength $\lambda = h\sqrt{[1/(2ME)]}$ and is striking an object of radius a . The scattering will be classical if $\phi \gg \lambda/(2\pi a)$. If we compare the particle size, a , with the Bohr radius, $a_0 = \hbar^2/(m_0 e^2)$, where m_0 , e are the electronic mass and charge, then

$$\frac{\lambda}{2\pi a_0} = \sqrt{\frac{e^2 m_0}{2a_0 M E}},$$

so classical mechanics will suffice if

$$E \gg \frac{e^2 m_0}{2a_0 M} \left(\frac{a_0}{a} \right)^2.$$

In practice this low energy limit is a fraction of an electron-volt in energy so even for small angle collisions ion implantation problems can be treated classically.

2.3 INTERATOMIC FORCES

Having decided that we can consider classical elastic collision events we must now choose a form for the repulsive potential between the ions in order to assign a finite radius to the particles and hence predict a scattering angle. Ideally one would choose a simple analytical expression for $V(r)$ and historically the Coulomb, Bohr and Born-Mayer potentials were of this form. Improvements to these functions were generally made by modifying factors rather than new functions. However, the successful descriptions of $V(r)$ over a wide range of ion separations have been made by numerical means. Such functions are now of value since computations are feasible with large modern computers. Figure 2.4 compares some of the alternative repulsive potentials which have been used and examples of analytical descriptions are given in Table 2.1. It is evident that the agreement between the curves extends over a limited range of separations. There is no definitive potential which is appropriate for all pairs of ions and all energies so even the simplest expressions contain empirically adjusted parameters. Comparison with experiment is difficult because elasticity and compressibility experiments only allow one

to sense the potential near the equilibrium atom spacing in the solid. The alternative is to probe the interaction in a dynamic event, i.e. by observing the scatter of an energetic ion beam. The principle is well established by the high energy alpha particle experiments of Rutherford (1911) to determine the size of the nuclei. Unfortunately ion implantation and radiation damage events involve the middle region of the potential curve which is the most difficult to characterise. One approach is to measure the scattering of ion beams from an inert gas and compare the results with an assumed potential. A recent review of this field was given by Kessel (1970).

An alternative approach is to use a computer simulation of a solid and compare ion range predictions with experiment. In principle one need only to assign initial positions to the ions, specify a repulsive potential between pairs of atoms and provide stability to the system by imposing a boundary condition which simulates the cohesive binding forces of the solid. When an energetic foreign atom "appears" in this system the lattice is perturbed and dynamic changes take place in the structure. However these can be followed by solving the classical equations of motion to find the new atomic positions after some small time increment. Iterative calculations of this type, coupled

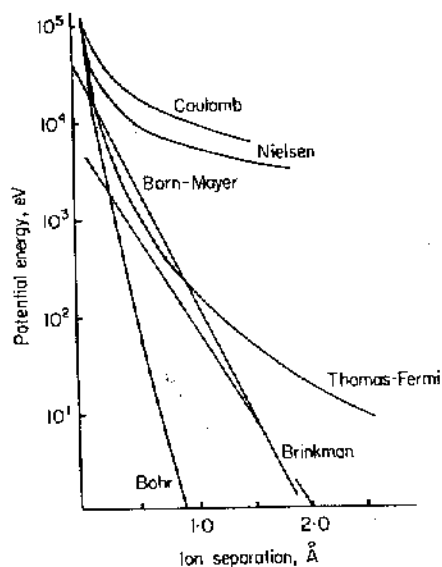


FIG. 2.4(a). A comparison of various proposed interatomic potentials between two copper atoms.

with computer printouts of the new positions, will display the development of radiation damage and the progress of the foreign ion. Suitable allowance for thermal energy will also show annealing of the radiation damage as the "lattice" relaxes to an equilibrium condition. Many events simulated in this way will produce a statistical view of the implantation process.

Such a computer program has the advantages that, once written, it allows one to explore variations in potentials or defect stability and obtain an overall impression of the changes. The limitations occur because one must use truncated or simplified potentials to minimise the computer running time and many mechanisms of energy dissipation will be ignored.

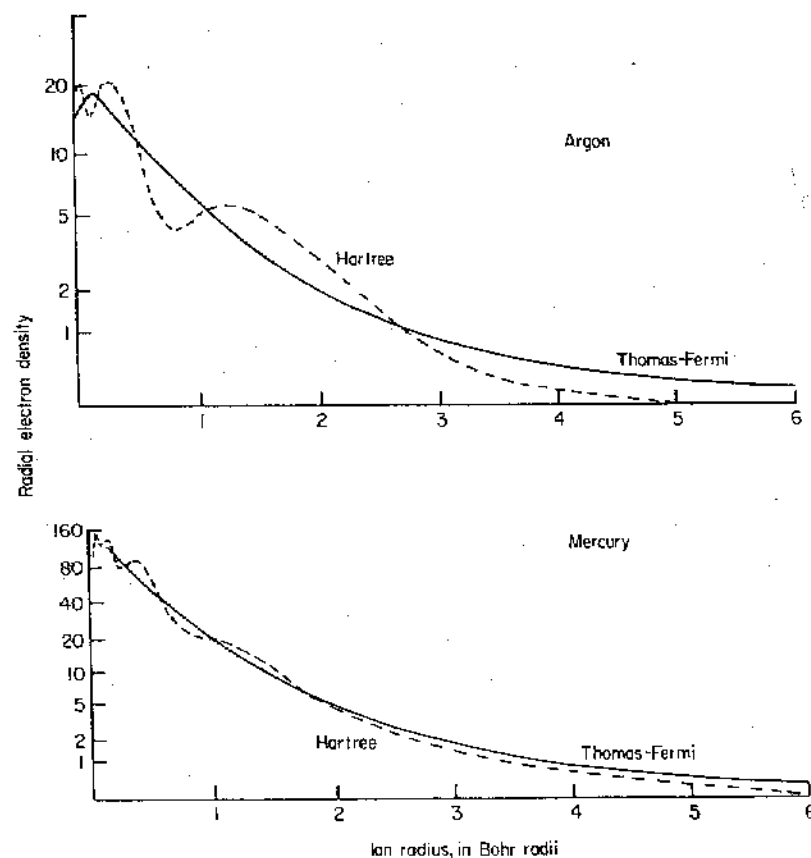


FIG. 2.4(b). Comparisons of the Thomas-Fermi and Hartree interatomic potentials for ions of argon and mercury.

TABLE 2.1 Examples of interatomic potentials.

Born-Mayer	$V(r) = A \exp\left(-\frac{r}{b}\right)$	A, b are constants
Coulomb	$V(r) = \frac{Z_1 Z_2 e^2}{r}$	
Neilson	$V(r) = \frac{Z_1 Z_2 e^2 a}{r^2} \exp(-1)$	where $a = \frac{a_0}{(Z_1 Z_2)^{1/6}}$ or $\frac{a_0}{(Z_1^{2/3} + Z_2^{2/3})^{1/2}}$
Screened Coulomb	$V(r) = \frac{Z_1 Z_2 e^2}{r} \exp\left(-\frac{r}{a}\right)$	a_0 being the first Bohr orbit.
Brinkman I	$V(r) = \frac{Z_1 Z_2 e^2}{r} \exp\left(-\frac{r}{a}\right) \left(\frac{1-r}{2a}\right)$	$a \sim a_0 (Z_1 Z_2)^{-1/6}$
Brinkman II	$V(r) = \frac{AZ_1 Z_2 e^2 \exp(-Br)}{1 - \exp(-Ar)}$	$A = \frac{0.95 \times 10^{-6}}{a_0} (Z_1 Z_2)^{7/4}$ $B = \frac{(Z_1 Z_2)^{1/6}}{1.5a_0}$
Firsov and LSS	$V(r) = \frac{Z_1 Z_2 e^2}{r} \phi_{TF}\left(\frac{r}{a}\right)$	$\phi_{TF}\left(\frac{r}{a}\right)$ is the Thomas-Fermi screening function.

Firsov and LSS theories use different forms of this function

Lindhard suggests

$$\phi_{TF}\left(\frac{r}{a}\right) = 1 - \left(\frac{r}{a}\right) \left[\left(\frac{r}{a}\right)^2 + 3 \right]^{-1/2}$$

whereas Firsov (1958) uses

$$\phi_{TF}\left(\frac{r}{a}\right) = \chi(Z_1^{1/2} + Z_2^{1/2})^{2/3} \left(\frac{r}{a}\right)$$

where the factor χ is tabulated by Gombas (1949).

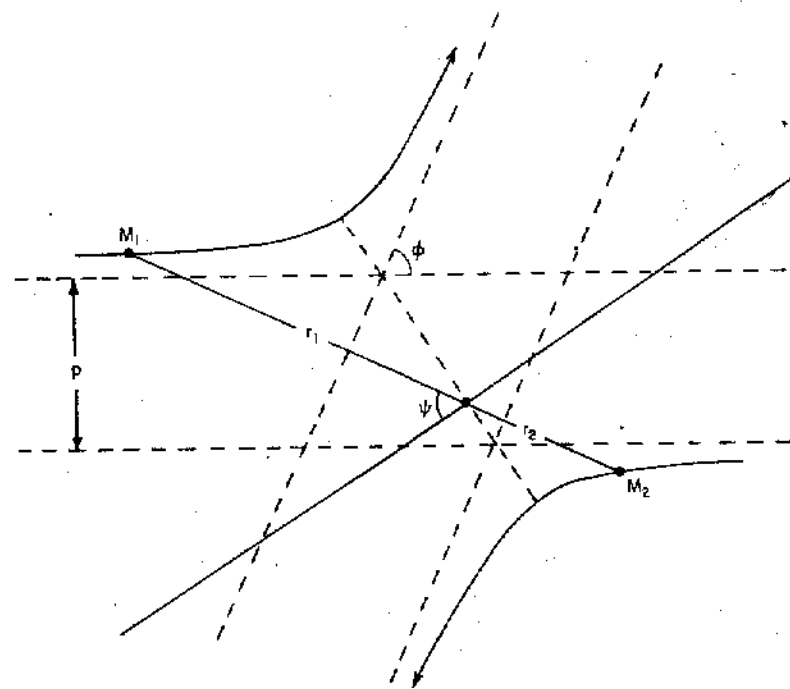


FIG. 2.5. The collision path in centre of mass co-ordinates.

2.4 SCATTERING DURING COLLISIONS

If we now consider ions of a finite size described by a potential function $V(r)$ then we are not limited to collisions where the line between the ion centres is also the direction of motion. Instead, off-axis collisions can be discussed in terms of an impact parameter, p , which is the perpendicular separation of the asymptotes of the hyperbolae which describe the ion trajectories in a centre of mass frame, Fig. 2.5. At any instant the distance of the ions from the centre of mass is

$$r_1 = \frac{M_2 r}{(M_1 + M_2)}, \quad \text{or} \quad r_2 = \frac{M_1 r}{(M_1 + M_2)},$$

where r is the pair separation. For these elastic collisions it is convenient to express the total energy as the sum of potential and kinetic energy with the

latter resolved parallel, and perpendicular, to the line between the ions. This gives,

$$\frac{M_2}{(M_1 + M_2)} E_1 = V(r) + \frac{1}{2} \frac{M_1 M_2}{(M_1 + M_2)} \left[\left(\frac{dr}{dt} \right)^2 + r^2 \left(\frac{d\psi}{dt} \right)^2 \right].$$

With finite atoms angular momentum is conserved hence

$$\frac{M_1 M_2}{(M_1 + M_2)} u_1 p = M_1 \left(\frac{r M_2}{M_1 + M_2} \right)^2 \frac{d\psi}{dt} + M_2 \left(\frac{r M_1}{M_1 + M_2} \right)^2 \frac{d\psi}{dt}.$$

By noting that

$$\left(\frac{dr}{dt} \right)^2 + r^2 \left(\frac{d\psi}{dt} \right)^2 = \left(\frac{d\psi}{dt} \right)^2 \left[\left(\frac{dr}{d\psi} \right)^2 + r^2 \right]$$

we can rearrange the energy expression to be independent of time. It is also customary to change variables at this point and write $u = r^{-1}$ so

$$\frac{du}{d\psi} = \left[\frac{1}{p^2} - \frac{V(u)}{E_1} \frac{(M_1 + M_2)}{M_2 p^2} - u^2 \right]^{\frac{1}{2}}.$$

But $d\psi$ is related to the total scattering angle ϕ by

$$\int_{\phi/2}^{\pi/2} d\psi = \frac{1}{2} (\pi - \phi)$$

or

$$\phi = \pi - 2p \int_0^{1/u_0} \left[1 - \frac{V(u)}{E_1} \frac{(M_1 + M_2)}{M_2} - p^2 u^2 \right]^{-\frac{1}{2}} du$$

where $1/u_0$ is the distance of closest approach ($R_1 + R_2$) if we consider an ion "radius".

This equation is important because if we can choose a potential $V(u)$, and integrate, then we can estimate the scattering. To compare the theory with experiment we cannot use the impact parameter so we introduce a differential cross section $d\sigma = 2\pi p dp$, which measures the area around the target atom from which a particular scattering angle would occur.

The total cross section for energy transfer

$$E_2 = T = \frac{4M_1 M_2 E_1}{(M_1 + M_2)^2} \sin^2 \left(\frac{\phi}{2} \right)$$

is

$$\sigma = \int_{T_{\min}}^{T_{\max}} \frac{d\sigma}{dE_2} dE_2.$$

Such a cross section equation measures both the energy losses for scattering and the energy transferred which can cause radiation damage. The lower limit of the integral should be chosen in different ways depending on whether we are considering energy loss for the slowing down of a primary or displacement of lattice atoms. In the latter case the lower limit is the threshold energy for removal of a lattice atom from its site.

For a particular scattering angle, the probability that the energy transfer is E_2 is related to the total cross section by

$$P(E_2) dE_2 = \frac{1}{\sigma} \frac{d\sigma}{dE_2} dE_2.$$

The mathematical problem of choosing a realistic $V(u)$ so that the scattering cross section can be evaluated is quite major. An extreme solution is to consider only glancing collisions where the direction of motion is essentially unchanged. This "impulse" or "momentum" approximation has the interesting result that T is proportional to E_1^{-1} irrespective of $V(u)$. At the other extreme one can use a hard sphere potential i.e.

$$V(r) = \infty \quad \text{for } r < R \\ = 0 \quad \text{for } r > R.$$

This gives $d\sigma \propto dT/T_{\max}$.

More realistic potentials can be used if we understand whether we are sensing a close or distant interaction of the ions. For example a Coulomb potential $V(r) = Z_1 Z_2 e^2 / r$ leads to $d\sigma \propto E_1 dT/T^2$ but is only appropriate for close penetration of the ions. The screened Coulomb potential used by Bohr (1948), $V(r) = Z_1 Z_2 e^2 / r \exp(-r/a_0)$ overcompensates and is too weak at large separations. A range of intermediate examples considered by Lindhard and his co-workers (1961, 1963) were power potentials of the form

$$V(r) \approx \frac{Z_1 Z_2 e^2}{r^s} \frac{a^{s-1}}{s},$$

where $a = 0.885 a_0 (Z_1^{2/3} + Z_2^{2/3})^{-1/2}$, these gave an elastic cross section

$$d\sigma \approx \frac{C_n}{T_{\max}^{1-1/s}} \frac{dT}{T^{(1+1/s)}} \quad \text{for } s > 1.$$

Here

$$C_n \approx \left(1 - \frac{1}{s} \right) \frac{\pi^2}{2.718} \frac{e^2 a_0 Z_1 Z_2 M_1}{(Z_1^{2/3} + Z_2^{2/3})^{1/2} (M_1 + M_2)}$$

reflects the underlying use of a modified classical Bohr atom. This cross section is also independent of primary energy in the case of an inverse square law potential, $s = 2$.

In attempts to find an analytic expression one is frequently making intelligent guesses at the form of the screening function. For example Firsov (1958) uses an expression

$$a = 0.885 a_0 (Z_1^{1/2} + Z_2^{1/2})^{-2/3}.$$

This differs from the preceding expression for the parameter a by 10 to 20%. Differences of this magnitude are of minor importance in the development of a range theory.

A variation of the inverse square potential is the Nielsen (1956) potential

$$V(r) = \frac{Z_1 Z_2 e^2 a_0}{r^2} \exp(-1).$$

It has the property that it intersects the screened Bohr potential at the value $r = a_0$. The major advantage of this potential is that Nielsen derives from it a quantitative measure of the total ion range, \bar{R} , as

$$\bar{R} = 0.6 \frac{(Z_1^{2/3} + Z_2^{2/3})^{1/2}}{Z_1 Z_2} \frac{(M_1 + M_2) M_2}{M_1} \frac{10^{-6} E}{D}$$

where D is the target density and E is measured in keV. Unfortunately it is only applicable for $M_1 > M_2$ and M_1, M_2 between 10 to 200. We shall also see (Section 2.6) that a prediction of the projected range would be preferable to the total range. However, as an easily evaluated first assessment of the range the above expression is useful.

The Lindhard, Scharff and Schiøtt (1963) potential used in most range calculations employs a Thomas-Fermi model of the atom to give

$$V(r) = \frac{Z_1 Z_2 e^2}{r} \phi_{TF} \left(\frac{r}{a} \right)$$

where the Thomas-Fermi function ϕ_{TF} is a numerical screening function. This has been tabulated by Gombas (1956) and a similar function used by Firsov (1958). Lindhard (1965) offers an approximate analytical form for ϕ_{TF} as

$$1 - \left(\frac{r}{a} \right) \left[\left(\frac{r}{a} \right)^2 + 3 \right]^{-1/2}.$$

Alternative power law expressions for the function are used by Winterbon *et al.* (1970) in the calculation of energy transfer to the target. It is therefore

essential to look more closely at the Thomas-Fermi potential and compare it with a more detailed electron density picture obtained by a Hartree or Hartree-Fock calculation. Figure 2.4(b) shows such a comparison for argon and mercury ions. It is clear that the Thomas-Fermi model represents the same total electronic charge but it has lost the detailed shell structure and will also produce a potential function which is too repulsive at large distance (i.e. > 3 Bohr radii for argon ions). Consequently calculations which use this potential will overestimate the energy loss at large ion separation. Hence ranges predicted by LSS theory are likely to be too short for heavy ions, which are intrinsically large, since the size of the Hartree and Thomas-Fermi ions will deviate most at large Z . Indeed Neilson *et al.* (1973) measure a range which is up to a factor of 2 greater than the predicted LSS range for heavy ions entering aluminium (see Section 2.11).

The LSS cross section for nuclear collisions is valuable because it is appropriate for all values of Z_1, Z_2, M_1, M_2 . It is therefore sensible to relate the cross section to dimensionless energy and range parameters ϵ and ρ ,

$$\epsilon = E \frac{a M_2}{Z_1 Z_2 e^2 (M_1 + M_2)}$$

$$\rho = R N M_2 \frac{4 \pi a^2 M_1}{(M_1 + M_2)^2}$$

where R is the range, and N the number of atoms per unit volume.

The stopping cross section, σ , is related to these parameters by

$$\left(\frac{d\epsilon}{d\rho} \right)_{\text{nuclear}} = \sigma \frac{(M_1 + M_2)}{4 \pi e^2 Z_1 Z_2 M_1}.$$

The universal curves computed from this expression are shown in Figures 2.6 and 2.7. In Figure 2.6 is plotted the differential cross section computed by LSS using a Thomas-Fermi model to give $d\sigma$ in terms of energy transfer t

$$d\sigma = \frac{\pi a^2}{2 t^{3/2}} f(t^{1/2}) dt$$

since

$$t = \epsilon^2 \sin^2 \left(\frac{\phi}{2} \right) = \epsilon^2 \left(\frac{T}{T_{\text{max}}} \right).$$

One can see that the LSS and Coulomb potentials predict the same scattering cross sections at high energies where we measure Rutherford scattering. In an intermediate energy range there is also some agreement with the cross section predicted by the inverse square potential.

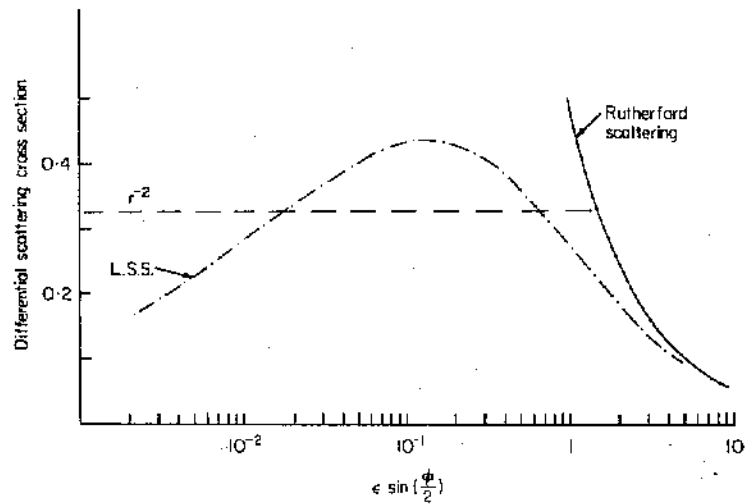


FIG. 2.6. The differential cross section for elastic nuclear collisions. The calculation from the LSS theory using a Thomas-Fermi potential approaches the Rutherford scattering cross section at high energy. For comparison the cross section for an inverse square law potential is also shown. The cross section and energy axes are plotted in terms of universal functions (see text).

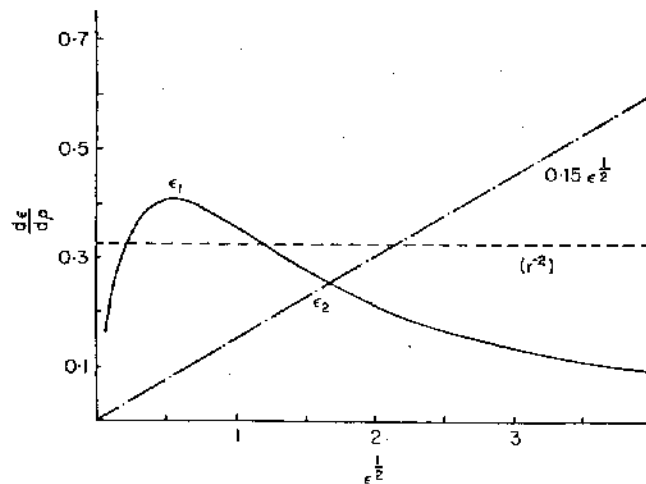


FIG. 2.7. Nuclear and electronic stopping cross sections in reduced units. The curved line is the nuclear cross section computed from the LSS theory of Fig. 2.6. Electronic stopping is proportional to velocity and for comparison the cross section for the inverse square law potential is also shown.

One should note that the differential cross section for nuclear collisions has taken on a general form because the changes produced by scaling the energy (and hence ϕ) are compensated by the $t^{1/2}$ term. An analytic form for $t^{1/2}$ is given by Winterbon *et al.* (1970, 1972) as

$$f(t^{1/2}) = \lambda t^{(1/2-m)} [1 + (2\lambda t^{(1-m)})^q]^{-1/q}$$

which approaches a power law, $\lambda t^{(1/2-m)}$, for small values of t . The parameters for this power law, λ , m and q are chosen empirically with λ and q being fairly constant, but the important exponent, m , is sensitive to the shape of the tail of the potential (i.e. small values of t).

The presentation of the universal cross section curve in terms of the cross section and velocity of the primary ion is shown in Fig. 2.7. Here the elastic (nuclear) energy losses are compared with the inelastic ones discussed in the next section.

To give some quantitative feel for the energies at which the nuclear cross section is a maximum, ϵ_1 , or the two processes are comparable, ϵ_2 , Tables 2.2 and 2.3 list some representative values of ϵ/E , ρ/R , ϵ_1 and ϵ_2 for a variety of ion target combinations. As a guide line we can equate ϵ_1 and ϵ_2 with ϵ values of 0.35 and 3.

In this section we have outlined how the Lindhard, Scharff, Schiøtt (1963) theory has developed; for a detailed discussion of the validity of this and other potentials the reader is referred to the books by Carter and Colligon (1968) and Torrens (1972), or the conference proceedings edited by Gehlen *et al.* (1972).

2.5 ELECTRONIC ENERGY LOSS

A classical approach is also appropriate when considering the inelastic energy loss from the passage of the ion through the electronic cloud of the target atom. Again one can trace the historical approach from the early theory of Bohr (1913) where he considered a fully ionised atom striking a second ion. The primary ion will be stripped of all its electrons if it is moving at a higher velocity than the electrons of the K shell ($v > Z_1 e^2/\hbar$) so the rate of energy loss will depend on the closeness of approach to the second atom and thus the number of electrons which can be excited. Bohr wrote the energy loss as

$$\left(\frac{dE}{dx}\right)_{\text{electronic}} = \frac{4\pi Z_1^2 e^4}{mv^2} B$$

where B is a measure of the penetration through the electron shells.